© Universiti Tun Hussein Onn Malaysia Publisher's Office

IJIE

http://penerbit.uthm.edu.my/ojs/index.php/ijie
ISSN : 2229-838X e-ISSN : 2600-7916

The International Journal of Integrated Engineering

Free Vibrational Behavior of Bi-Directional Functionally Graded Composite Panel with and Without Porosities Using 3D Finite Element Approximations

Pankaj S. Ghatage[1,2], P. Edwin Sudhagar[1*]

[1]School of Mechanical Engineering,
Vellore Institute of Technology, Vellore - 632014, Tamilnadu, INDIA

[2]Department of Automobile Engineering, Rajarambapu Institute of Technology, Rajaramnagar,
Affiliated to Shivaji University, Kolhapur, Islampur - 415414, Maharashtra, INDIA

*Corresponding Author

DOI: https://doi.org/10.30880/ijie.2023.15.01.012
Received 14 August 2021; Accepted 11 October 2021; Available online 28 February 2023

Abstract: The frequency characteristics of bi-directional functionally graded (FG) rectangular panels with and without porosities are examined in this work using 3D finite element approximations. The properties of graded panel consist metal and ceramic material varied smoothly in bi-direction. The material properties of this highly heterogeneous material are obtained using the Voigt material model and Power-law. The present model is developed using a customized computer code and discretized using three-dimensional solid 20-noded quadrilateral elements. The mesh refinement is conducted to present the convergence test. The validation test is presented by showing comparison of the obtained findings with the results reported in the previous literature. At a later stage, comprehensive parametric research is presented through numerical illustrations which reveal that the geometrical and material parameters of bi-directional functionally graded panel affect its frequency characteristics, significantly. Finally, the developed 3D FEM model to predict the free vibrational characteristics of multidirectional FG rectangular plates with and without porosities will be the reference for the continuation of research in this area.

Keywords: Bi-directional FGMs, free vibration, finite element approximation

1. Introduction

Recently, multidirectional functionally graded composite materials show significant improvement in their characteristics, which results in attracting considerable attention in aerospace as well as other engineering application because of their enormous advantages over laminated composites and unidirectional functionally graded materials (FGMs). Koizumi [1] had proposed the idea of FGM in Japan for producing thermal barrier materials, in the 19^{th} century many researchers had contributed to the development of unidirectional FGMs but some modern structures like advanced space crafts, shuttles, etc. demand advanced FGMs, whose micromechanical properties should vary not only in one direction but also vary in two or more than two directions and hence the concept of multidirectional FGMs was introduced in plate structure in which the micromechanical properties graded in two or more than two directions from one surface to another. FGM structures are typically composed of a grouping of metal and ceramic, metals exhibit good strength and toughness while ceramic materials are having good anti-oxidant as well as thermal resistance behavior. Free vibrational behavior of plate structure is one of the important concerns for structural designers; hence various researches have been conducted to evaluate the free vibrational behavior of FGM structures [27-29], whereas in recent decades, a group of researchers has worked to model and analyze multi-directional FGM structures [2-10].

*Corresponding author: edwinsudhagar.p@vit.ac.in

The free vibrational behavior of multidirectional FG annular plates using the differential quadrature method (DQM) presented by Nie and Zhong [3]. The micromechanical material properties are graded in two directions. It was observed that the free vibrational behavior of the multi-directional FG plate was different than the unidirectional FG plate. Kermani et al. [4] carry forwarded the same study by changing geometry and boundary conditions to predict free vibrational behavior. The findings revealed that multi-directional FGMs influence natural frequencies as well as mode shapes of the plate. Nejati et al. [5] analyzed the free vibrational behavior of bi-directional FG annular plates with the DQM. The multi-directional FG piezoelectric annular plates were analyzed and presented vibrational behavior using DQM by Yas and Moloudi [9]. The buckling as well as vibrational responses of 2D-FG circular plate considering uniform plane load resting on the elastic foundation was presented by Ahlawat and Lal [11]. Further, Lal and Ahlawat [12] investigated the buckling and vibrational response of circular plates of 2D-FG materials by considering a hydrostatic in-plane force. Mahinzare et al. [13] developed a model to analyze the free vibrational behavior of 2D FG micro circular plate using the FSDT. Van Do et al. [14] presented buckling and bending responses of 2D-FG plates using the finite element approximation. Lieu et al. [15] have studied the bending and vibration behavior of in-plane 2D-FG plates considering the variable thickness. Ahlawat [16] presented the buckling and vibrational responses of 2D-FG circular plates. Ghatage et al. [17] have presented the first time, a review on multidirectional FG composite structures including its modeling and analysis. Esmaeilzadeh and Kadkhodayan [18] studied a dynamic response of porous 2D-FG plates using a dynamic relaxation method. Wu and Yu [19] analyzed the free vibrational responses of 2D-FGM annular plates with the help of a finite annular prism method in which they presented the impact of different boundary conditions on the free vibrational behavior of plates. Liu and Cheng [20] proposed a systematic approach of voxel modeling and analysis for FGM structures in the Ansys environment. Kandasamy et al. [21] simulated the FGMs structures using APDL codes and compared the buckling and vibrational responses of the FG structure with findings of existing methods. Ersoy et al. [22] proposed the approximate numerical solution to predict free vibrational characteristics of FG annular plates and shells structures using two different approaches and the findings are compared with results generated by using ANSYS packed program. Huang et al. [23] analyzed the buckling behavior of FGM rings using FSDT and the findings are compared to the results obtained by the ABAQUS commercial software. Higher-order finite element models developed by researchers to forecast the vibrational, flexural, and buckling responses of FG structures [39-44]. Thai and Kim [25] presented a review on different methods of modeling and analysis of FGM panels.

During the production of FG structures, the porosities usually form in the structure. Wattanasakulpong et al. [31] experimentally proved that the static and dynamic analysis of FGM panels by considering porosities claims more accurate results, hence structural behavior of FGM structure need be analyzed by considering porosities. Many authors contributed to analyzing FG structure considering porosities [31-37]. Sobhy and Zenkour [32] presented the influence of porosities on the vibrational and buckling behavior of FG nanoplate using quasi three-dimensional refined theory. Wang and Zu [33] carried out the vibrational responses of unidirectional FGM plates considering porosities with the thermal environments. Wattanasakulpong and Ungbhakorn [34] presented nonlinear and linear vibrational responses of unidirectional FGM elastically restrained ends beams with porosities. Barati and Shahverdi [35] considered even and uneven porosity pattern to analyze the stability of supersonic FGM panels in different fields. Even and uneven porosity distribution was also considered to analyze vibrations of longitudinal traveling unidirectional FG plates by Wang et al. [36]. In the open literature, only Karamanli and Aydogdu [37] considered two-directional even porosity distributions to carry out structural dynamics and stability behavior of 2D-FGM micro-sized beams using modified coupled stress theory.

From available multi-directional FG plate literature, one can notice that most of the researchers have worked on multi-directional FG circular as well as annular plates; however, the rectangular plates are widely used in different engineering applications. Swaminathan et al. [45] stated that additional focus is needed to develop numerical techniques for 3D analysis of FG structures in order to reduce computing time and cost. Also based on open literature, this is the first attempt, in which free vibrational analysis of bi-directional FG rectangular plates (BFGRP) with various porosity pattern using the 3D elasticity theory was studied. So, in this present work, the frequency characteristics of the BFGRP with and without porosities are examined using the finite element approximation in combination with the 3D elasticity theory. The material properties of this highly heterogeneous material are obtained using the Voigt model via extended Power-law. The proposed model is developed using a customized computer code and discretized using three-dimensional solid 20-noded quadrilateral elements. The mesh refinement is confirmed with convergence test and validation test also confirmed by comparing the current work with previously reported work. The effects different parameters like as thickness ratio (a/h), boundary conditions, aspect ratio (a/b) and an impact of even as well as uneven porosities of multi-directional FG plate on natural frequency are presented in this work.

2. Effective Material Properties (EMP) of FGM

In this research work, FG rectangular plates with length 'a', width 'b' and thickness 'h' are taken in to account in the system of cartesian coordinates i.e., x, y, and z, which is depicted in Fig. 1(a). The EMP of 2D-FGM are graded in x and y direction with Power-law material distribution. The EMP can be represented as;

$$EMP = \sum_{j=1}^{k} P_j V_{f_j} \tag{1}$$

where, P_j is the material properties and V_{f_j} represents the volume fractions

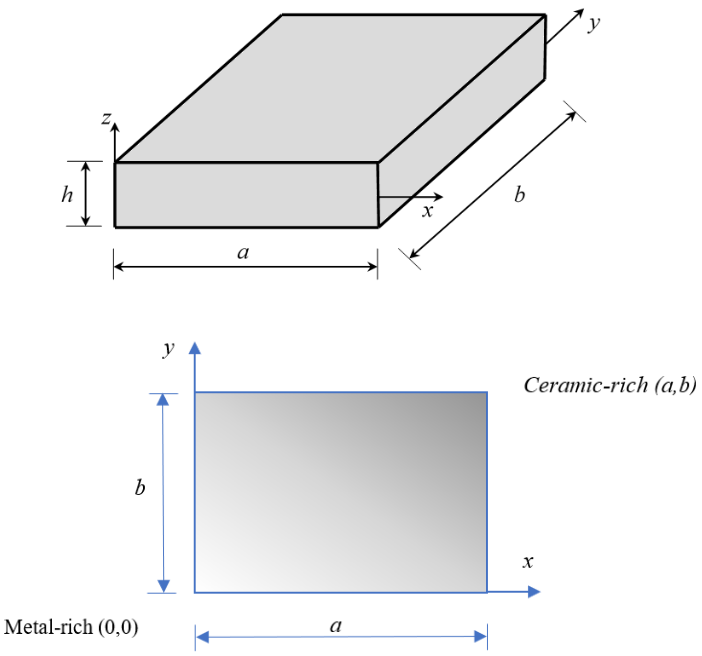

Fig. 1 (a) - Representation of 2D-FG rectangular plate

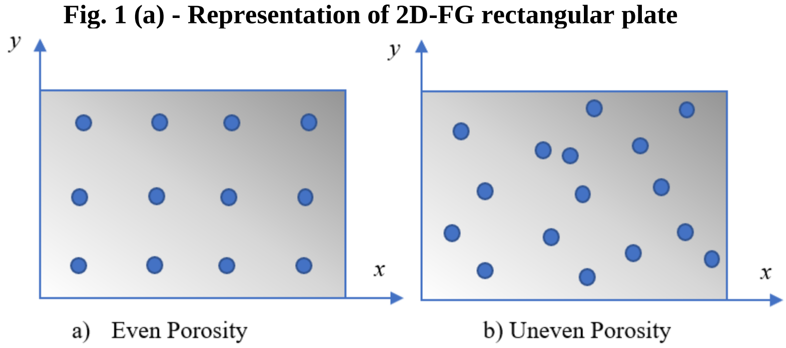

Fig. 1 (b) - Representation of porosity distribution

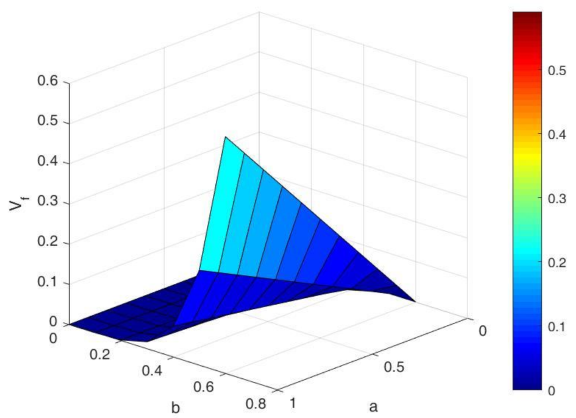

Fig. 2 - Distribution of volume fraction profile of BFGRP with n_x =1, n_y =5

The volume fraction based on Power-law function can be obtained as per equation (2) [18]. The volume fraction distribution profiles of bidirectional FG plate are depicted in Fig. 2 and Fig. 3.

$$V_f = \left(\frac{x}{a}\right)^{n_x} \left(\frac{y}{b}\right)^{n_y} \left. \begin{matrix} 0 \le n_x < \infty \\ 0 \le n_y < \infty \end{matrix} \right\} \tag{2}$$

where, n_x and n_y are the indices of Power-law in x and y directions, respectively.

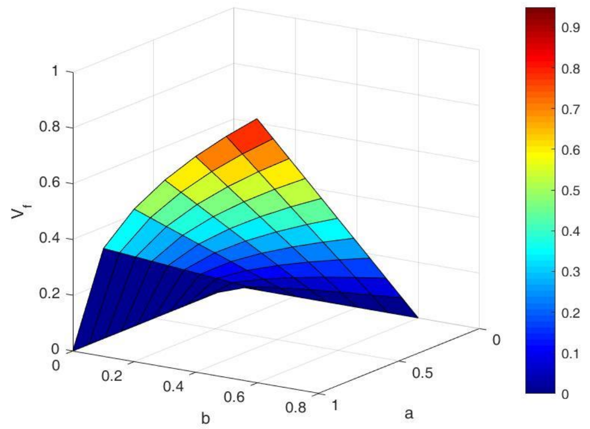

Fig. 3 - Distribution volume fraction profile of BFGRP with n_x =1, n_y =0.5

The EPM like Young's modulus (*E*), mass density (ρ) and Poisson's ratio (v) of bi-directional FGM are calculated by equations (3-5) [38].

$$E = (E_c - E_m)V_f + E_m \tag{3}$$

$$\rho = (\rho_c - \rho_m)V_f + \rho_m \tag{4}$$

$$v = (v_c - v_m)V_f + v_m \tag{5}$$

Fig. 1(b) represents the even and uneven porosity pattern in the FG rectangular plate. The EPM of 2D-FGM plate with even porosity pattern can be calculated using equation (6-8) and the EPM of 2D-FGM plate with uneven porosity pattern in bi-direction expressed as in equations (9-11) [36].

$$E = (E_c - E_m)V_f + E_m - \frac{\alpha}{2}(E_c + E_m) \tag{6}$$

$$\rho = (\rho_c - \rho_m)V_f + \rho_m - \frac{\alpha}{2}(\rho_c + \rho_m) \tag{7}$$

$$v = (v_c - v_m)V_f + v_m - \frac{\alpha}{2}(v_c + v_m) \tag{8}$$

$$E = (E_c - E_m)V_f + E_m - \frac{\alpha}{2}(E_c + E_m)\left(1 - \frac{2|x|}{a}\right) \tag{9}$$

$$\rho = (\rho_c - \rho_m)V_f + \rho_m - \frac{\alpha}{2}(\rho_c + \rho_m)\left(1 - \frac{2|x|}{a}\right) \tag{10}$$

$$v = (v_c - v_m)V_f + v_m - \frac{\alpha}{2}(v_c + v_m)\left(1 - \frac{2|x|}{a}\right) \tag{11}$$

Where, α $(\alpha << 1)$ is the porosity volume fraction.

3. Mathematical Formulation

To obtain the free vibrational responses of BFGRP, the problem is formulated using 3D elasticity theory and finite element approximation.

3.1 Governing Equations

The governing equations of motion for the BFGRP in Cartesian coordinate system are depicted in equations (12-14) [26, 30]. The displacements *u*, *v*, and *w* along *x*, *y* and *z* direction respectively. ρ represents the mass density which depends on *x* and *y* coordinates.

$$\frac{\partial \sigma_{xx}}{\partial x} + \frac{\partial \sigma_{xy}}{\partial y} + \frac{\partial \sigma_{zx}}{\partial z} = \rho(x, y)\frac{\partial^2 u}{\partial t} \tag{12}$$

$$\frac{\partial \sigma_{xy}}{\partial x} + \frac{\partial \sigma_{yy}}{\partial y} + \frac{\partial \sigma_{yz}}{\partial z} = \rho(x, y)\frac{\partial^2 v}{\partial t} \tag{13}$$

$$\frac{\partial \sigma_{xz}}{\partial x} + \frac{\partial \sigma_{yz}}{\partial y} + \frac{\partial \sigma_{zz}}{\partial z} = \rho(x, y)\frac{\partial^2 w}{\partial t} \tag{14}$$

3.2 Stress Strain Relations

The generalised stress-strain relationship can be expressed in terms of its reference plane using Hook's law as in equation (15) [30]

$$\{\sigma\} = [Q]\{\varepsilon\} \tag{15}$$

where, $\{\sigma\} = \{\sigma_{xx} \quad \sigma_{yy} \quad \sigma_{zz} \quad \tau_{xy} \quad \tau_{yz} \quad \tau_{xz}\}^T$ and $\{\varepsilon\} = \{\varepsilon_{xx} \quad \varepsilon_{yy} \quad \varepsilon_{zz} \quad \gamma_{xy} \quad \gamma_{yz} \quad \gamma_{xz}\}^T$ are the stress and strain vector respectively and $[Q]$ is the rigidity matrix as shown in equation (16).

$$[Q] = \frac{E(1-v)}{(1+v)(1-2v)}\begin{bmatrix} Q_{11} & Q_{12} & Q_{13} & 0 & 0 & 0 \\ Q_{21} & Q_{22} & Q_{23} & 0 & 0 & 0 \\ Q_{31} & Q_{32} & Q_{33} & 0 & 0 & 0 \\ 0 & 0 & 0 & Q_{44} & 0 & 0 \\ 0 & 0 & 0 & 0 & Q_{55} & 0 \\ 0 & 0 & 0 & 0 & 0 & Q_{66} \end{bmatrix} \tag{16}$$

Where,

$$Q_{11} = Q_{22} = Q_{33} = 1, \quad Q_{12} = Q_{23} = Q_{13} = \frac{v}{(1-v)}, \; Q_{44} = Q_{55} = Q_{66} = \frac{1-2v}{2(1-v)}$$

3.3 Relations of Strain-Displacement

The strain-displacement relations for rectangular Cartesian coordinates in a three-dimensional elasticity theory can be stated as follows [30];

$$\left.\begin{aligned} &\varepsilon_{xx} = \frac{\partial u}{\partial x},\ \varepsilon_{yy} = \frac{\partial v}{\partial y}, \varepsilon_{zz} = \frac{\partial w}{\partial z}, \gamma_{xz} = \left(\frac{\partial u}{\partial y} + \frac{\partial v}{\partial x}\right) \\ &\gamma_{yz} = \left(\frac{\partial v}{\partial z} + \frac{\partial w}{\partial y}\right), \gamma_{zx} = \left(\frac{\partial w}{\partial x} + \frac{\partial u}{\partial z}\right) \end{aligned}\right\} \tag{17}$$

Three-dimensional strain-displacement correlation can be expressed as;

$$\varepsilon = B\delta \tag{18}$$

Where the differential operator *B* and displacement δ is defined as in equation (19) and (20) respectively, the differential operator *B* and displacement δ contribute to develop the three-dimensional strain. Also, the displacement δ indicates the degree of freedom.

$$B = \begin{bmatrix} \frac{\partial}{\partial x} & 0 & 0 \\ 0 & \frac{\partial}{\partial y} & 0 \\ 0 & 0 & \frac{\partial}{\partial z} \\ 1/2\frac{\partial}{\partial y} & 1/2\frac{\partial}{\partial x} & 0 \\ 0 & 1/2\frac{\partial}{\partial z} & 1/2\frac{\partial}{\partial y} \\ 1/2\frac{\partial}{\partial z} & 0 & 1/2\frac{\partial}{\partial x} \end{bmatrix} \tag{19}$$

$$\delta = \begin{Bmatrix} u \\ v \\ w \end{Bmatrix} \tag{20}$$

3.4 Finite Element Formulation

A three-dimensional 20-noded solid higher-order element with three degrees of freedom for each node in rectangular cartesian coordinates is considered for discretization in this investigation. As indicated in equation (21), displacements can be represented in terms of shape functions.

$$\delta = \sum_{i=1}^{20} N_i \delta_i \tag{21}$$

Equations (22) and (23) express the nodal displacement vector of the element δ_i and the shape function matrix N_i respectively.

$$\delta_i = \left\{ U_1 \;\; V_1 \;\; W_1 \ldots\ldots U_{20} \;\; V_{20} \;\; W_{20} \right\}^T \tag{22}$$

$$N_i\left(\xi,\eta,\zeta\right) = \begin{bmatrix} N_1 & 0 & 0 & N_2 & 0 & 0 & . & . & . & N_{20} & 0 & 0 \\ 0 & N_1 & 0 & 0 & N_2 & 0 & . & . & . & 0 & N_{20} & 0 \\ 0 & 0 & N_1 & 0 & 0 & N_2 & . & . & . & 0 & 0 & N_{20} \end{bmatrix} \tag{23}$$

ξ, η and ζ are the natural coordinates in *x*, *y* and *z* directions respectively. The shape function terms are depicted in an appendix. The components of shape function can be represented in the form of natural coordinates as per equation (24).

$$N_i\left(\xi,\eta,\zeta\right) = \frac{1}{8}\left(1+\xi_i\xi\right)\left(1+\eta_i\eta\right)\left(1+\zeta_i\zeta\right) \tag{24}$$

Hamilton principle is used to compute governing equations as shown in equation (25)

$$\int_0^T (\partial U - \partial T)dT = 0 \tag{25}$$

Where, ∂U represents virtual strain energy per unit volume and ∂T represents kinetic energy per unit volume which are expressed in equation (26-28).

$$U = \frac{1}{2}\int_v \{\sigma\}^T \{\varepsilon\} dv = \frac{1}{2}\int_v \{\delta\}^T [B]^T [Q][B]\{\delta\} dv \tag{26}$$

$$U = \frac{1}{2}\{\delta\}^T [K]\{\delta\} \tag{27}$$

$$T = \frac{1}{2}\int_v \rho \{\delta\}^T \{\delta\} dv = \frac{1}{2}\int_A \{\delta\}^T [M]\{\delta\} dA \tag{28}$$

$$[M][\ddot{\delta}] + [K][\delta] = 0 \tag{29}$$

Where, $[\ddot{\delta}]$ is the second derivative of nodal displacement and $[\delta]$ is the nodal displacement.
The variational method was used to derive the elemental stiffness matrix $[K]$ and the mass matrix $[M]$, which are stated as;

$$[K] = \int_{-1}^{+1}\int_{-1}^{+1}\int_{-1}^{+1} [B]^T [Q][B]|J| d\xi d\eta d\zeta \tag{30}$$

$$[M] = \int_{-1}^{+1}\int_{-1}^{+1}\int_{-1}^{+1} [N]^T [m][N]|J| d\xi d\eta d\zeta \tag{31}$$

where, $|J|$ is the determinant of the Jacobian matrix used for the mapping, $[N]$ is the shape function matrix and $[m]$ is the elemental inertia matrix.
The free vibration behaviour is obtained by equation (32).

$$\left([K] - \omega^2 [M]\right)\Delta = 0 \tag{32}$$

Where, $[K]$ global stiffness matrix and $[M]$ global mass matrix. ω represents natural frequency and Δ is the respective eigen-vectors.

4. Convergence and Validation Study

To obtain the free vibrational behavior of a BFGRP using the proposed model, it is essential to confirm the precision and effectiveness of the developed model. This is ensured by studying convergence and validation test, which is discussed below with two different examples;

Example I:

To study the convergence, free vibration analysis of BFGRP is presented with $n_x = 0.5, n_y = 0.5$, aspect ratio $a/b = 1.5$ and thickness ratio $a/h = 10$. BFGRP is assumed to be constituted with Stainless Steel and Silicon Nitride; FGM constituent's properties are depicted in Table 1. The non-dimensional frequency (NDF) responses are obtained by using equation $\bar{\omega} = (\omega a^2 / h)\left(\sqrt{\rho_c / E_c}\right)$, which is exhibited in Fig. 4, the five modes of vibration presented in the figure. Based on convergence study, the non-dimensional frequency parameters of 18 × 18 × 18 mesh size have been found good convergence and the average percentage difference between results of 18 × 18 × 18 and 20 × 20 × 20 mesh size is less than 0.2%, hence it is suitable for the free vibrational analysis of BFGRP.

Table 1 - FGM component's properties [24]

Materials	Properties		
	Density $\rho\ (kg/m^3)$	**Poisson's Ratio** ν	**Young's Modulus** $E(GPa)$
Stainless steel (SUS304)	8166	0.3177	207.78
Silicon nitride (Si_3N_4)	2370	0.24	322.27

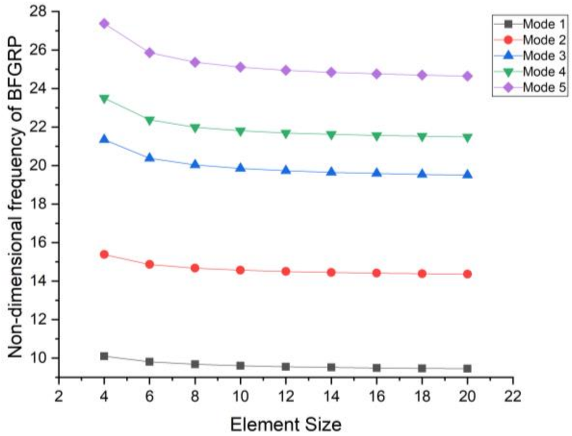

Fig. 4 - Convergence test of non-dimensional linear frequency for clamped (CCCC) BFGRP (SUS304/ Si_3N_4) for $n_x = 0.5, n_y = 0.5$, $a/b = 1.5$ and $a/h = 10$.

Example II: In this illustration, the free vibrational analysis of simply supported (SSSS) square FG plate with Power-law indices $(n_z = 0,\ 0.5,\ 1, 5, 10, \infty)$ and thickness ratio $a/h = 10$ is discussed, the NDF parameters using equation $\bar{\omega} = (\omega a^2 / h)\left(\sqrt{\rho_c / E_c}\right)$ are presented. The plate is comprised with Stainless Steel and Silicon Nitride material; Table 1 lists the properties of the same. To verify the precision of the current model, the findings of the present model are compared with the findings of Talha and Singh [24] as shown in Fig. 5. It is observed that the percentage difference between computed results and the results of Talha and Singh [24] is within 5%. The results obtained using the current model match well with the findings of Talha and Singh [24].

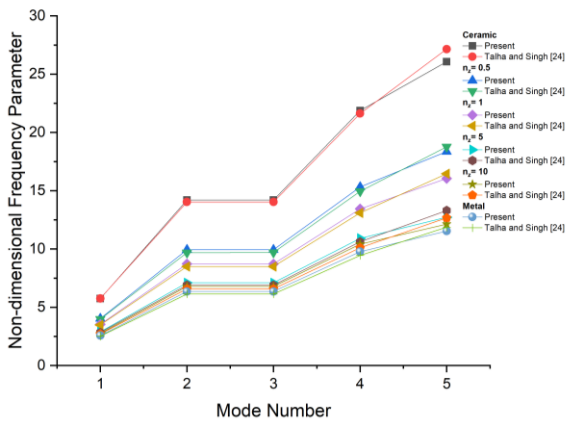

Fig. 5 - NDF responses of SSSS square FG (SUS304/ Si_3N_4) plates

5. Result and Discussions

Free vibration analysis of BFGRP using customized computer codes is presented and discussed in this section. To explore the effectiveness of the developed model, the influence of thickness ratio, aspect ratio, boundary conditions and the influence of porosities of BFGRP on natural frequency are discussed with some new examples.

5.1 Effect of Thickness Ratio

Table 2 shows that the effect of thickness ratio (*a/h*) on NDF parameter $\bar{\omega} = (\omega a^2 / h)\left(\sqrt{\rho_c / E_c}\right)$ of fully clamped (CCCC) rectangular plate with four different materials (Ceramic, FGM-I, FGM-II, and Metal) and aspect ratio (a/b) is 1.5. The plate is comprised with Stainless Steel and Silicon Nitride material; Table 1 lists the properties of the same. The natural frequency should rise as the thickness ratio of the plate increases; nevertheless, the opposite tendency is found in the current investigation due to the representation of NDF characteristics. The ceramic plates are having more non-dimensional frequency compare to other material plates moreover, the bi-directional FGM-II plates are having less non-dimensional frequency than bidirectional FGM-I, so it noticed that increase in volume fraction index in certain direction reduces the NDF parameter, hence FGM -II is having less stiffness compare to FGM-I. It is anticipated that approximately 4% fall in NDF parameter for FGM-II compare to FGM-I.

Table 2 - Effect of thickness ratio on the NDF parameter of BFGRP

Material	n_x	n_y	a/h	Modes									
				1	2	3	4	5	6	7	8	9	10
Ceramic	0	0	10	15.7433	23.1472	33.9435	34.5562	39.7612	43.1520	48.6081	49.1092	51.8658	56.6246
			20	17.5849	26.6511	41.2058	41.4601	49.0100	60.9762	62.0053	73.9844	79.5224	80.9125
			50	18.2552	28.0779	44.3638	44.5631	53.3621	67.1748	68.6269	83.1804	90.0692	91.7692
			100	18.3582	28.3172	44.8784	45.1154	54.1191	68.3063	69.8527	84.8211	92.0898	93.7925
FGM-I	1	5	10	7.1006	10.8174	15.1441	16.4065	18.4077	19.8615	23.1736	23.1903	23.2630	25.0859
			20	7.9280	12.4349	18.3889	19.6325	22.6790	29.0974	29.2353	32.7980	37.1592	37.9524
			50	8.2291	13.0904	19.8038	21.0752	24.6874	32.0032	32.3265	36.9038	42.1762	42.8228
			100	8.2752	13.2000	20.0344	21.3314	25.0347	32.5345	32.8955	37.6371	43.1132	43.7695
FGM-II	10	5	10	6.9001	10.3168	14.7825	15.5536	17.5537	19.1400	21.9402	22.0081	22.6278	24.6166
			20	7.7038	11.8605	17.9395	18.6098	21.6110	27.5068	27.6415	32.1568	35.5481	35.8046
			50	7.9953	12.4837	19.3111	19.9676	23.5122	30.2278	30.5484	36.1495	40.2984	40.3630
			100	8.0397	12.5863	19.5339	20.2052	23.8390	30.7187	31.0759	36.8618	41.1777	41.2359
Metal	∞	∞	10	6.8592	10.1772	14.7157	15.2486	17.3274	18.8808	21.4774	21.5043	22.5006	24.5196
			20	7.6608	11.7172	17.8630	18.2886	21.3491	26.9055	27.1339	32.0329	34.9867	35.1311
			50	7.9516	12.3401	19.2300	19.6457	23.2374	29.6055	30.0096	36.0121	39.4767	39.8323
			100	7.9961	12.4435	19.4520	19.8841	23.5626	30.0958	30.5339	36.7212	40.3410	40.7030

5.2 Effect of Aspect Ratio

Fig. 6 shows the effect of aspect ratio (*a/b*) on NDF parameters $\overline{\omega} = (\omega a^2 / h)\left(\sqrt{\rho_c / E_c}\right)$ of fully clamped (CCCC) rectangular plate with four different materials (Ceramic, FGM-I, FGM-II, and Metal) and thickness ratio (a/b) is 10. The plate is comprised with Stainless Steel and Silicon Nitride material; Table 1 lists the properties of the same. The NDF parameters are computed for ten different modes. It is noticed that the NDF parameter is increased with an increase in aspect ratio and mode number as anticipated. It is observed that, average approximately 50% rise in frequency parameter when aspect ratio changes from 1 to 2.5. Also, the NDF parameter of the bidirectional FGM plate decreases by approximately 3% when the material of the plate changes from FGM-I to FGM-II.

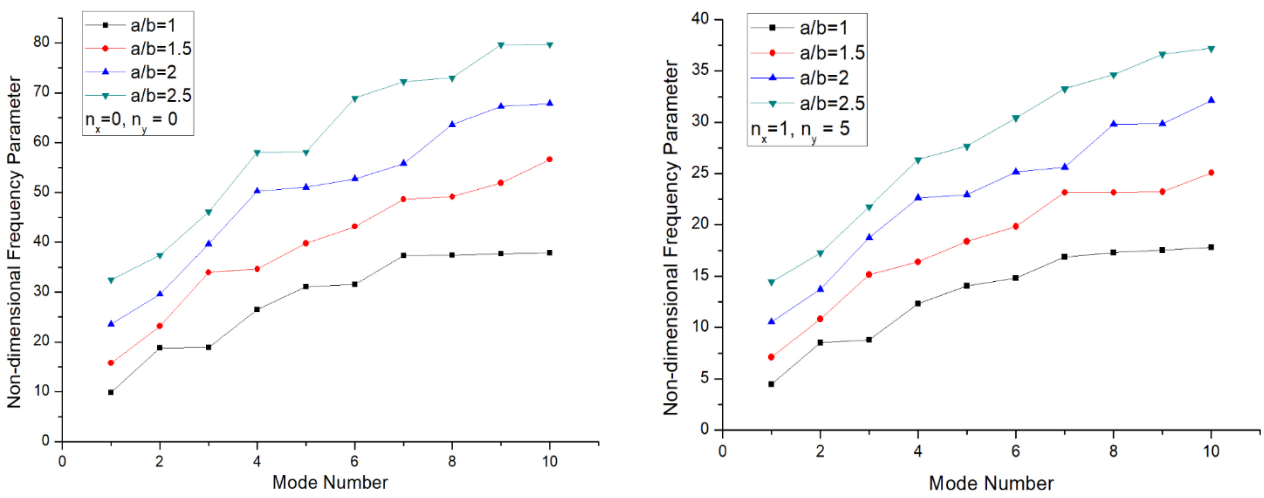

(a) Ceramic Rectangular Plates

(b) FGM-I Rectangular Plates

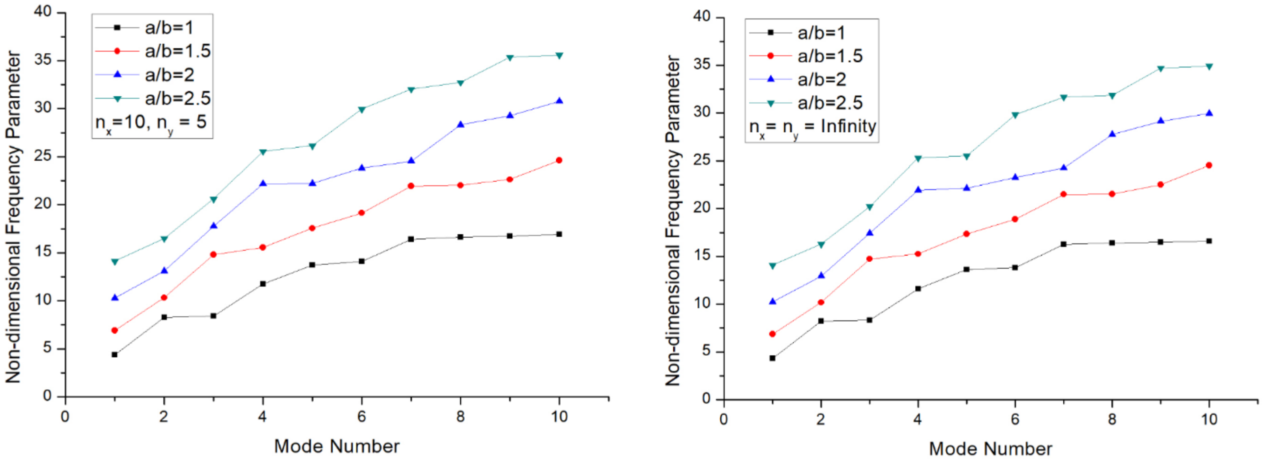

(c) FGM-II Rectangular Plates (b) Metallic Rectangular Plates

Fig. 6 - Effect of aspect ratio on the NDF parameter of BFGRP

5.3 Effect of Boundary Condition

Table 3 shows that the effect of different boundary conditions on the NDF parameter $\overline{\omega} = (\omega a^2 / h)\left(\sqrt{\rho_c / E_c}\right)$ of fully simply supported (SSSS), fully clamped (CCCC), simply supported clamped (SCSC) and cantilever (CFFF) rectangular plate with four different materials (Ceramic, FGM-I, FGM-II, and Metal). The aspect ratio (a/b) and thickness ratio (a/h) of the plates are considered as 1.5 and 10 respectively. The plate is comprised with Stainless Steel and Silicon Nitride material; Table 1 lists the properties of the same. For all materials, the lowest frequency is recorded for plates with CFFF boundary condition and the highest frequency is recorded for plates with CCCC boundary condition, and the frequency ranges of SSSS and SCSC boundary conditions are in between the frequencies of CCCC and CFFF. The NDF responses increase with the increase in constraint on the boundaries of the BFGRP. The average difference between the non-dimensional frequency of CCCC and CFFF is approximately 70%.

Table 3 - Effect of different boundary condition on the NDF parameter of BFGRP

Material	n_x	n_y	B.C.	Modes									
				1	2	3	4	5	6	7	8	9	10
Ceramic	0	0	SSSS	13.6047	20.7516	24.7933	27.0935	30.2311	31.5382	32.6471	35.3256	38.8511	43.5324
			CCCC	15.7481	23.1671	33.9430	34.5907	39.7763	43.1628	48.6474	49.1302	51.8674	56.6193
			SCSC	11.6536	19.6750	20.6864	27.4120	28.7229	31.0021	32.8309	33.3406	42.3998	43.5690
			CFFF	1.0339	3.2621	5.3077	6.1523	10.6304	14.6877	15.8192	16.5887	17.4610	20.5657
FGM-I	1	5	SSSS	6.1496	9.7209	11.9721	12.8110	13.4899	15.0153	15.1915	16.3898	19.7871	20.6465
			CCCC	7.0957	10.8071	15.1328	16.3871	18.3829	19.8394	23.1520	23.1574	23.2264	25.0697
			SCSC	5.2929	9.2014	9.2289	12.2609	13.5540	14.7594	15.4922	15.4949	20.0958	20.7074
			CFFF	0.5513	1.6605	2.7481	3.0764	5.4868	7.4977	7.7908	8.1421	8.4255	10.4590
FGM-II	10	5	SSSS	5.9744	9.2666	11.5442	12.4899	13.1790	14.2453	14.5988	15.6398	18.7289	19.5640
			CCCC	6.9001	10.3168	14.7825	15.5536	17.5537	19.1400	21.9402	22.0081	22.6278	24.6166
			SCSC	5.1374	8.8027	9.0662	11.9602	12.9990	14.0088	14.7788	14.9323	19.0619	20.1066
			CFFF	0.5073	1.5431	2.5494	2.9384	5.1503	7.0305	7.3339	7.7795	8.0672	9.9191
Metal	∞	∞	SSSS	5.9367	9.1346	11.3357	12.2813	13.1144	13.9431	14.4027	15.4216	18.0823	19.1448
			CCCC	6.8592	10.1772	14.7157	15.2486	17.3274	18.8808	21.4774	21.5043	22.5006	24.5196
			SCSC	5.0998	8.6750	9.0220	11.8972	12.7781	13.7130	14.5670	14.7017	18.6550	19.5980
			CFFF	0.4838	1.4880	2.4482	2.8568	4.9529	6.7945	7.1254	7.6173	7.8835	9.6120

5.4 Effect of Porosities

The effect of even and uneven porosities on the NDF parameter $\overline{\omega} = (\omega a^2 / h)\left(\sqrt{\rho_c / E_c}\right)$ of fully clamped (CCCC) BFGRP with four different FGM (FGM, FGM-I, FGM-II, and FGM-III) is presented in tabular form as shown in Table 4 and 5 respectively. The aspect ratio (a/b) and thickness ratio (a/h) of the plates are considered as 1.5 and 10 respectively. The plate is comprised with Stainless Steel and Silicon Nitride material; Table 1 lists the properties of the same. It is clear from the obtained results that the fundamental NDF parameter shows a decreasing trend with an increase in porosity volume fraction in even type of porosity, however it shows an increasing trend in uneven distribution of porosity. The value of the NDF parameter of BFGRP with uneven porosity pattern is higher than the even porosity pattern, hence the uneven distribution of porosities increases the stiffness of the plate. It is noticed that approximately 4% rise in NDF in a plate with uneven porosities compare to plate with even porosities when porosity volume fraction is 0.1 and that rise in NDF parameter increases up to 15% when porosity volume fraction is 0.3.

Table 4 - Effect of even porosities on the NDF parameter of BFGRP

Material	n_x	n_y	α	Modes									
				1	2	3	4	5	6	7	8	9	10
FGM	1	0.5	0	8.6147	13.2016	17.8619	19.8550	22.5809	23.7399	27.0844	27.9901	28.3592	28.7606
			0.1	8.4897	13.0912	17.5036	19.7149	22.3325	23.4037	26.5154	27.7940	28.0930	28.1647
			0.2	8.3312	12.9462	17.0569	19.5339	22.0017	22.9753	25.8095	27.2244	27.5919	27.8996
			0.3	8.1249	12.7506	16.4879	19.2892	21.5480	22.4128	24.9129	26.1888	27.2638	27.5197
FGM-I	1	5	0	7.1006	10.8174	15.1441	16.4065	18.4077	19.8615	23.1736	23.1903	23.2630	25.0859
			0.1	6.8775	10.5070	14.6457	15.9518	17.8457	19.2666	22.4149	22.5178	22.6218	24.2437
			0.2	6.6156	10.1444	14.0621	15.4232	17.1970	18.5775	21.5243	21.7484	21.8869	23.2539
			0.3	6.2950	9.6966	13.3466	14.7675	16.3958	17.7299	20.4332	20.7931	20.9709	22.0437
FGM-II	10	5	0	6.9001	10.3168	14.7825	15.5536	17.5537	19.1400	21.9402	22.0081	22.6278	24.6166
			0.1	6.6728	9.9919	14.2841	15.0740	16.9815	18.5295	21.2452	21.3362	21.8686	23.7814
			0.2	6.4006	9.6029	13.6887	14.4986	16.2966	17.7989	20.4111	20.5285	20.9607	22.7835
			0.3	6.0693	9.1271	12.9629	13.7933	15.4593	16.9060	19.3895	19.5371	19.8528	21.5668
FGM-III	100	100	0	6.8592	10.1772	14.7157	15.2486	17.3274	18.8808	21.4774	21.5043	22.5006	24.5196
			0.1	6.6286	9.8437	14.2146	14.7540	16.7449	18.2520	20.7818	20.7931	21.7349	23.6817
			0.2	6.3532	9.4450	13.6155	14.1618	16.0493	17.4993	19.9391	19.9488	20.8200	22.6811
			0.3	6.0170	8.9579	12.8859	13.4382	15.2001	16.5800	18.8964	18.9304	19.7047	21.4612

Table 5 - Effect of uneven porosities on the NDF parameter of BFGRP

Material	n_x	n_y	α	Modes									
				1	2	3	4	5	6	7	8	9	10
FGM	1	0.5	0	8.6147	13.2016	17.8619	19.8550	22.5809	23.7399	27.0844	27.9901	28.3592	28.7606
			0.1	8.6244	13.2060	17.8608	19.8243	22.5760	23.8336	27.0924	27.9114	28.3069	28.7488
			0.2	8.6341	13.2092	17.8597	19.7957	22.5712	23.9236	27.1005	27.8392	28.2568	28.7369
			0.3	8.6432	13.2119	17.8587	19.7682	22.5663	24.0098	27.1081	27.7730	28.2094	28.7245
FGM-I	1	5	0	7.1006	10.8174	15.1441	16.4065	18.4077	19.8615	23.1736	23.1903	23.2630	25.0859
			0.1	7.1162	10.8454	15.1495	16.4286	18.4260	19.9628	23.1941	23.1989	23.2630	25.0778
			0.2	7.1356	10.8809	15.1646	16.4669	18.4670	20.0797	23.2286	23.2431	23.2970	25.0842
			0.3	7.1539	10.9143	15.1786	16.5019	18.5053	20.1912	23.2609	23.2840	23.3277	25.0896
FGM-II	10	5	0	6.9001	10.3168	14.7825	15.5536	17.5537	19.1400	21.9402	22.0081	22.6278	24.6166
			0.1	6.9271	10.3696	14.8170	15.6231	17.6221	19.2876	22.0254	22.0906	22.6940	24.6580
			0.2	6.9519	10.4186	14.8483	15.6872	17.6873	19.4272	22.1040	22.1665	22.7544	24.6936
			0.3	6.9756	10.4639	14.8763	15.7460	17.7477	19.5592	22.1773	22.2360	22.8093	24.7232
FGM-III	100	100	0	6.8592	10.1772	14.7157	15.2486	17.3274	18.8808	21.4774	21.5043	22.5006	24.5196
			0.1	6.8888	10.2381	14.7578	15.3359	17.4120	19.0489	21.5905	21.6169	22.5825	24.5794
			0.2	6.9163	10.2942	14.7955	15.4157	17.4896	19.2052	21.6935	21.7177	22.6558	24.6279
			0.3	6.9416	10.3459	14.8289	15.4879	17.5618	19.3523	21.7867	21.8098	22.7215	24.6683

6. Conclusions

The free vibrational behaviour of 2D-FG fully clamped rectangular plate is reported in this work using 3D-FEM. The EMP of the FGM are obtained the using Voigt model in connection with the Power-law function. Convergence and validation tests are presented to ensure the accuracy of the proposed model. From the convergence study, it is found that (18×18x18) mesh is suitable to obtain the NDF responses. The validation test reveals that the proposed model agrees well with previously reported results. The influence of thickness ratio, aspect ratio and boundary conditions of the 2D-FGM on NDF parameters presented also the results of the 2D-FGM plates are compared with the ceramic and metal rectangular plates. Finally, the impacts of thickness ratio, aspect ratio, and boundary conditions on NDF characteristics of 2D-FG plate are observed to be substantial. Following is some concluding remarks observed through parametric study;

1. The plates with ceramic material reported the highest non-dimensional frequency parameters compare to the other materials because the ceramic material is having high stiffness. Moreover, the FGM-I is stiffer than FGM-II.
2. The natural frequency should be increased as the thickness ratio of the plate increases; however, the opposite trend is detected in the present study due to the exhibition of NDF characteristics.
3. The non-dimensional frequency responses of BFGRP rise with increasing plate aspect ratio and mode number as expected.
4. The highest frequency responses are observed for bi-directional FG graded plates with CCCC boundary conditions, while the lowest frequency responses are recorded for CFFF boundary conditions. The frequency responses rise as the BFGRP become more constrained
5. The fundamental non-dimensional frequency of BFGRP declines with a rise in porosity volume fraction in even type of porosity, however it shows an increasing trend in uneven distribution of porosity. The FG plates with uneven porosity pattern are stiffer than plates with even porosity pattern.
6. The developed 3D-FEM model for free vibrational analysis of multidirectional FG rectangular panels with and without porosities will be the reference for the continuation of research in this area. Also, this approach can be further extended for the irregular geometries however, the computational time and cost will be increased.

Declaration of conflicting interests

The author(s) declared no potential conflicts of interest with respect to the research, authorship, and/or publication of this article.

Appendix

Shape function terms

$$N_1=\frac{1}{8}(u_1(1-\xi)(1-\eta)(1-\zeta)(-\xi-\eta-\zeta-2)) \qquad N_{11}=\frac{1}{4}(u_{11}(1-\xi^2)(1+\eta)(1-\zeta))$$

$$N_2=\frac{1}{8}(u_2(1+\xi)(1-\eta)(1-\zeta)(\xi-\eta-\zeta-2)) \qquad N_{12}=\frac{1}{4}(u_{12}(1-\xi)(1-\eta^2)(1-\zeta))$$

$$N_3=\frac{1}{8}(u_3(1+\xi)(1+\eta)(1-\zeta)(\xi+\eta-\zeta-2)) \qquad N_{13}=\frac{1}{4}(u_{13}(1-\xi^2)(1-\eta)(1+\zeta))$$

$$N_4=\frac{1}{8}(u_4(1-\xi)(1+\eta)(1-\zeta)(-\xi+\eta-\zeta-2)) \qquad N_{14}=\frac{1}{4}(u_{14}(1+\xi)(1-\eta^2)(1+\zeta))$$

$$N_5=\frac{1}{8}(u_5(1-\xi)(1-\eta)(1+\zeta)(-\xi-\eta+\zeta-2)) \qquad N_{15}=\frac{1}{4}(u_{15}(1-\xi^2)(1+\eta)(1+\zeta))$$

$$N_6=\frac{1}{8}(u_6(1+\xi)(1-\eta)(1+\zeta)(\xi-\eta+\zeta-2)) \qquad N_{16}=\frac{1}{4}(u_{16}(1-\xi)(1-\eta^2)(1+\zeta))$$

$$N_7=\frac{1}{8}(u_7(1+\xi)(1+\eta)(1+\zeta)(\xi+\eta+\zeta-2)) \qquad N_{17}=\frac{1}{4}(u_{17}(1-\xi)(1-\eta)(1-\zeta^2))$$

$$N_8=\frac{1}{8}(u_8(1-\xi)(1+\eta)(1+\zeta)(-\xi+\eta+\zeta-2)) \qquad N_{18}=\frac{1}{4}(u_{18}(1+\xi)(1-\eta)(1-\zeta^2))$$

$$N_9=\frac{1}{4}(u_9(1-\xi^2)(1-\eta)(1-\zeta)) \qquad N_{19}=\frac{1}{4}(u_{19}(1+\xi)(1+\eta)(1-\zeta^2))$$

$$N_{10}=\frac{1}{4}(u_{10}(1+\xi)(1-\eta^2)(1-\zeta)) \qquad N_{20}=\frac{1}{4}(u_{20}(1-\xi)(1+\eta)(1-\zeta^2))$$

References

[1] Koizumi, M. F. G. M. (1997). FGM activities in Japan. Composites Part B: Engineering, 28(1-2),1-4.

[2] Alipour, M. M., Shariyat, M., & Shaban, M. (2010). A semi-analytical solution for free vibration of variable thickness two-directional-functionally graded plates on elastic foundations. International Journal of Mechanics and Materials in Design, 6(4), 293-304.

[3] Nie, G., & Zhong, Z. (2010). Dynamic analysis of multi-directional functionally graded annular plates. Applied Mathematical Modelling, 34(3), 608-616.

[4] Kermani, I. D., Ghayour, M., & Mirdamadi, H. R. (2012). Free vibration analysis of multi-directional functionally graded circular and annular plates. Journal of Mechanical science and Technology, 26(11), 3399-3410.
[5] Nejati, M., Mohsenimonfared, H., & Asanjarani, A. (2015). Free vibration analysis of 2D functionally graded annular plate considering the effect of material composition via 2D differential quadrature method. Mechanics of Advanced Composite Structures, 2(2), 95-111.
[6] Nie, G., & Zhong, Z. (2007). Axisymmetric bending of two-directional functionally graded circular and annular plates. Acta Mechanica Solida Sinica, 20(4), 289-295.
[7] Shariyat, M., & Mohammadjani, R. (2013). Three-dimensional compatible finite element stress analysis of spinning two-directional FGM annular plates and disks with load and elastic foundation non-uniformities. Latin American Journal of Solids and Structures, 10(5), 859-890.
[8] Shariyat, M., & Mohammadjani, R. (2014). Three-dimensional stress field analysis of rotating thick bidirectional functionally graded axisymmetric annular plates with nonuniform loads and elastic foundations. Journal of Composite Materials, 48(23), 2879-2904.
[9] Yas, M. H., & Moloudi, N. (2015). Three-dimensional free vibration analysis of multi-directional functionally graded piezoelectric annular plates on elastic foundations via state space-based differential quadrature method. Applied Mathematics and Mechanics, 36(4), 439-464.
[10] Zafarmand, H., & Kadkhodayan, M. (2015). Three-dimensional elasticity solution for static and dynamic analysis of multi-directional functionally graded thick sector plates with general boundary conditions. Composites Part B: Engineering, 69, 592-602.
[11] Ahlawat, N., & Lal, R. (2016). Buckling and vibrations of multi-directional functionally graded circular plate resting on elastic foundation. Procedia Engineering, 144, 85-93.
[12] Lal, R., & Ahlawat, N. (2017). Buckling and vibrations of two-directional functionally graded circular plates subjected to hydrostatic in-plane force. Journal of Vibration and Control, 23(13), 2111-2127.
[13] Mahinzare, M., Barooti, M. M., & Ghadiri, M. (2018). Vibrational investigation of the spinning bi-dimensional functionally graded (2-FGM) micro plate subjected to thermal load in thermal environment. Microsystem Technologies, 24(3), 1695-1711.
[14] Van Do, T., Nguyen, D. K., Duc, N. D., Doan, D. H., & Bui, T. Q. (2017). Analysis of bi-directional functionally graded plates by FEM and a new third-order shear deformation plate theory, Thin-Walled Structures, 119, 687-699.
[15] Lieu, Q. X., Lee, S., Kang, J., & Lee, J. (2018). Bending and free vibration analyses of in-plane bi-directional functionally graded plates with variable thickness using isogeometric analysis. Composite Structures, 192, 434-451.
[16] Ahlawat, N. (2019). Numerical solution for buckling and vibration of bi-directional FGM circular plates. AIP Conference Proceedings, 2061(1), 020020.
[17] Ghatage, P. S., Kar, V. R., & Sudhagar, P. E. (2020). On the numerical modelling and analysis of multi-directional functionally graded composite structures: A review. Composite Structures, 236, 111837.
[18] Ebrahimi, M. J., & Najafizadeh, M. M. (2014). Free vibration analysis of two-dimensional functionally graded cylindrical shells, Applied Mathematical Modelling, 38(1), 308-324.
[19] Wu, C. P., & Yu, L. T. (2019). Free vibration analysis of bi-directional functionally graded annular plates using finite annular prism methods. Journal of Mechanical Science and Technology, 33(5), 2267-2279.
[20] Liu, W., & Cheng, X. (2018). A systematic approach based on voxel modelling and APDL analysis for Functional-Graded-Material objects. Procedia CIRP, 78, 138-143.
[21] Kandasamy, R., Dimitri, R., & Tornabene, F. (2016). Numerical study on the free vibration and thermal buckling behavior of moderately thick functionally graded structures in thermal environments. Composite Structures, 157, 207-221.
[22] Tekieli, M., De Santis, S., de Felice, G., Kwiecień, A., & Roscini, F. (2017). Application of Digital Image Correlation to composite reinforcements testing. Composite Structures, 160, 670-688.
[23] Huang, H., Zhang, Y., & Han, Q. (2017). Stability of hydrostatic-pressured FGM thick rings with material nonlinearity. Applied Mathematical Modelling, 45, 55-64.
[24] Talha, M., & Singh, B. N. (2010). Static response and free vibration analysis of FGM plates using higher order shear deformation theory. Applied Mathematical Modelling, 34(12), 3991-4011.
[25] Thai, H. T., & Kim, S. E. (2015). A review of theories for the modeling and analysis of functionally graded plates and shells. Composite Structures, 128, 2015, 70-86.
[26] Asemi, K., Salami, S. J., Salehi, M., & Sadighi, M. (2014). Dynamic and static analysis of FGM skew plates with 3D elasticity based graded finite element modeling, Latin American Journal of Solids and Structures, 11(3), 504-533.
[27] Kar, V. R., & Panda, S. K. (2017). Large-amplitude vibration of functionally graded doubly-curved panels under heat conduction. AIAA Journal, 55(12), 4376-4386.

[28] Kar, V. R., Panda, S. K., & Pandey, H. K. (2018). Numerical study of temperature dependent eigenfrequency responses of tilted functionally graded shallow shell structures. Structural Engineering and Mechanics, 68(5), 527-536.
[29] Kar, V. R., & Panda, S. K. (2013). Free vibration responses of functionally graded spherical shell panels using finite element method. Gas Turbine India Conference, 35161, 2013, V001T05A014
[30] Loy, C. T., & Lam, K. Y. (1999). Vibration of thick cylindrical shells on the basis of three-dimensional theory of elasticity. Journal of sound and Vibration, 226(4), 719-737.
[31] Wattanasakulpong, N., Prusty, B. G., Kelly, D. W., & Hoffman, M. (2012). Free vibration analysis of layered functionally graded beams with experimental validation. Materials & Design (1980-2015), 36, 182-190.
[32] Sobhy, M., & Zenkour, A. M. (2019). Porosity and inhomogeneity effects on the buckling and vibration of double-FGM nanoplates via a quasi-3D refined theory. Composite Structures, 220, 289-303.
[33] Wang, Y. Q., & Zu, J. W. (2017). Vibration behaviors of functionally graded rectangular plates with porosities and moving in thermal environment. Aerospace Science and Technology, 69, 550-562.
[34] Wattanasakulpong, N., & Ungbhakorn, V. (2014). Linear and nonlinear vibration analysis of elastically restrained ends FGM beams with porosities. Aerospace Science and Technology, 32(1), 111-120.
[35] Barati, M. R., & Shahverdi, H. (2017). Aero-hygro-thermal stability analysis of higher-order refined supersonic FGM panels with even and uneven porosity distributions. Journal of Fluids and Structures, 73, 125-136.
[36] Wang, Y. Q., Wan, Y. H., & Zhang, Y. F. (2017). Vibrations of longitudinally traveling functionally graded material plates with porosities. European Journal of Mechanics-A/Solids, 66, 55-68.
[37] Karamanli, A., & Aydogdu, M. (2019). Structural dynamics and stability analysis of 2D-FG microbeams with two-directional porosity distribution and variable material length scale parameter. Mechanics Based Design of Structures and Machines, 48(2), 164-191.
[38] Adineh, M., & Kadkhodayan, M. (2017). Three-dimensional thermo-elastic analysis of multi-directional functionally graded rectangular plates on elastic foundation. Acta Mechanica, 228(3), 881-899.
[39] Chaudhary, S. K., Kar, V. R., & Shukla, K. K. (2021). Flexural Behavior of Perforated Functionally Graded Composite Panels under Complex Loading Conditions: Higher-Order Finite-Element Approach. Journal of Aerospace Engineering, 34(6), 04021081.
[40] Kar, V. R., Mahapatra, T. R., & Panda, S. K. (2017). Effect of different temperature load on thermal postbuckling behaviour of functionally graded shallow curved shell panels. Composite Structures, 160, 1236-1247.
[41] Karakoti, A., & Kar, V. R. (2019). Deformation characteristics of sinusoidally-corrugated laminated composite panel–A higher-order finite element approach. Composite Structures, 216, 151-158.
[42] Kar, V. R., & Panda, S. K. (2016). Post-buckling behaviour of shear deformable functionally graded curved shell panel under edge compression. International Journal of Mechanical Sciences, 115, 318-324.
[43] Kar, V. R., & Panda, S. K. (2017). Postbuckling analysis of shear deformable FG shallow spherical shell panel under nonuniform thermal environment. Journal of Thermal Stresses, 40(1), 25-39.
[44] Joshi, K. K., & Kar, V. R. (2021). Effect of material heterogeneity on the deformation behaviour of multidirectional (1D/2D/3D) functionally graded composite panels. Engineering Computations.
[45] Swaminathan, K., Naveenkumar, D. T., Zenkour, A. M., & Carrera, E. (2015). Stress, vibration and buckling analyses of FGM plates—A state-of-the-art review. Composite Structures, 120, 10-31.